HHS Public Access

Author manuscript

J Mol Biol. Author manuscript; available in PMC 2023 October 15.

Published in final edited form as:

J Mol Biol. 2022 October 15; 434(19): 167755. doi:10.1016/j.jmb.2022.167755.

Structural mechanism of TAF-Iβ chaperone function on linker histone H1.10

Haniqao Feng[1], **Bing-Rui Zhou**[1], **Charles D. Schwieters**[2], **Yawen Bai**[1,*]

[1]Laboratory of Biochemistry and Molecular Biology, Center for Cancer Research, National Cancer Institute, National Institutes of Health, Bethesda, MD 20892, USA

[2]Laboratory of Chemical Physics, National Institute of Diabetes and Digestive and Kidney Diseases, National Institutes of Health, Bethesda, MD 20892, US

Abstract

Linker histone H1, facilitated by its chaperones, plays an essential role in regulating gene expression by maintaining chromatin's higher-order structure and epigenetic state. However, we know little about the structural mechanism of how the chaperones recognize linker histones and conduct their function. Here, we used biophysical and biochemical methods to investigate the recognition of human linker histone isoform H1.10 by the TAF-Iβ chaperone. Both H1.10 and TAF-Iβ proteins consist of folded cores and disordered tails. We found that H1.10 formed a complex with TAF-Iβ in a 2:2 stoichiometry. Using distance restraints obtained from methyl-TROSY NMR and spin labels, we built a structural model for the core region of the complex. In the model, the TAF-Iβ core interacts with the globular domain of H1.10 mainly through electrostatic interactions. We confirmed the interactions by measuring the effects of mutations on the binding affinity. A comparison of our structural model with the chromatosome structure shows that TAF-Iβ blocks the DNA binding sites of H1.10. Our study provides insights into the structural mechanism whereby TAF-Iβ functions as a chaperone by preventing H1.10 from interacting with DNA directly.

Graphical Abstract

*Correspondence to Yawen Bai, baiyaw@mail.nih.gov.

Yawen Bai: Conceptualization, Data analysis, Visualization, Manuscript Writing, Supervision. **Hanqiao Feng:** Conceptualization, Data curation, Data analysis, Writing-Methodology. **Bing-Rui Zhou:** Data curation, Writing-Methodology. **Charles D. Schwieters:** Software, Writing-Methodology.

Author contributions

Y.B. and H.F. initiated the project. H.F. conducted the experiments and computational modeling. C.D.S. assisted with the use of Xplor-NIH. B-R.Z. performed chaperone function experiment. Y.B. and H.F. wrote the paper.

Declarations of interest: none

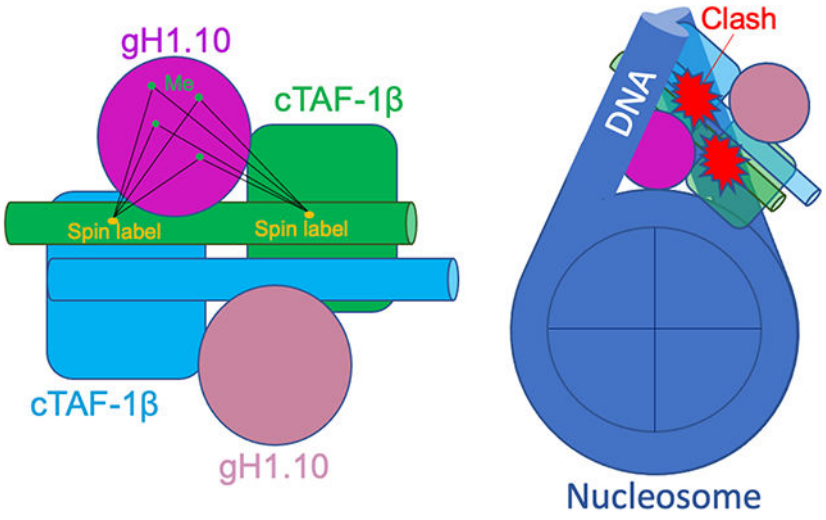

Keywords

Linker histone H1; TAF-Iβ; Histone chaperone; Methyl-TROSY; Spin label; Nucleosome; Chromatosome

Introduction

Linker histone H1, along with the core histones, associates with the genomic DNA to form the chromatosome, the repeating structural unit of metazoan chromatin [1-3]. H1 plays essential roles in a variety of cellular functions [4, 5], including gene expression [6, 7], mitotic chromosome architecture and segregation [8], muscle differentiation [9], embryonic stem cell differentiation [10], the genetic activity of heterochromatin [11], and cell pluripotency [12]. Loss of linker histones can lead to the change of epigenetic landscape and structural decompaction of chromatin [13], driving cancer cell heterogeneity [14] and lymphoma [15]. Also, mutations in linker histones are associated with autism and premature aging [16, 17].

In humans, linker histones have 11 isoforms (variants or subtypes); seven of them are expressed in somatic cells (from H1.0 to H1.5, and H1.10 (H1x)), and four (from H1.6 to H1.9) in germ cells [18]. The somatic H1s have a conserved tripartite structure consisting of a short flexible N-terminal tail, a central globular domain, and a long, intrinsically disordered, highly basic C-terminal tail. The short N-terminal tail of linker histones generally contributes little to nucleosome binding. Instead, the middle globular domain preferentially binds to the nucleosome dyad and linker DNAs [19]. On the other hand, the long C-terminal tail is essential for higher-affinity binding of linker histones to the nucleosome [20], linker DNA dynamics [21], and higher-order structures of chromatin [22].

Histones are positively charged proteins associated primarily with DNA and their chaperones *in vivo*. Various core histone chaperons have been identified, and the structures of some chaperones bound to the core histones have been determined at high resolution [23]. However, only few proteins have been shown to have the chaperone functions for linker

histones, including ProTα [24], TAF-1β [25], NAP1 [26], and NASP [27]. Furthermore, no structures of the chaperones bound to the linker histones have been determined. In the case of ProTα, which is an intrinsically disordered protein (IDP), it remains disordered when associated with the linker histone [28].

TAF-Iβ (Template activating factor-Iβ), which stimulates Adenovirus core DNA replication [29], is a multi-functional protein. It is initially identified as a translocation breakpoint-encoded protein in acute undifferentiated leukemia [30]. TAF-Iβ is a subunit of the INHAT complex that inhibits the activity of histone acetyltransferases [31] and binds to core histones with a chaperone activity [32, 33]. TAF-Iβ consists of a short N-terminal region, a folded middle region, and an extended C-terminal region with almost exclusively Asp and Glu residues (Fig. 1A). The crystal structure of TAF-Iβ shows that the folded core region forms a homodimer with a "headphone-like" shape [33]. The acidic C-terminal tail of TAF-Iβ is essential for its linker histone chaperone activity and enhancement of H1 fluidity, but not for H1 binding [25]. TAF-Iβ binds to linker histone H1 in the mammalian somatic cell nucleus, affects the exchange kinetics of H1 in living Hela cells, and displays linker histone chaperone activity by facilitating chromatosome formation *in vitro* [25]. Paradoxically, TAF-Iβ can also enhance transcription by evicting H1 from chromatin reconstituted with H1 [34].

In this study, we showed that the linker histone H1.10 (Fig. 1B) binds to the homodimeric TAF-Iβ with 2:2 stoichiometry. Using methyl-TROSY NMR and paramagnetic spin labels on the core region of TAF-Iβ (cTAF-Iβ), we obtained the distances between the methyl groups of the globular domain of H1.10 (gH1.10) and the spin labels, allowing us to build a structural model for the gH1.10-cTAF-Iβ complex. We further verified the model and investigated its functional implications through mutation studies.

Results

TAF-Iβ binds to H1.10 in a 2:2 stoichiometry

Previous studies have shown that TAF-Iβ specifically associates with linker histone isoform H1.10 in mammalian somatic cell nuclei and regulates its dynamics as a chaperone [25]. To investigate the structure of H1.10 bound to TAF-Iβ, we expressed and purified recombinant H1.10 and TAF-Iβ (Fig. 1C) (see Materials and methods). We performed size exclusion experiments on the full-length H1.10-TAF-Iβ and gH1.10-cTAF-Iβ complexes with different ratios (Fig. S1) and measured the molecular weights of the peaks at the smallest elusion volume using size exclusion chromatography and multi-angle light scattering (SEC-MALS) (Fig. 1D, E). The results showed a dimer of TAF-Iβ bound to two H1.10 molecules for both full-length proteins and folded core domains.

Methyl-TROSY NMR and Spin labeling

Our attempt to crystalize the H1.10-TAF-1β or gH1.10-cTAF-1β complex was unsuccessful. We also failed to see the particles of the H1.10-TAF-1β complex with sufficient resolution by cryo-EM, likely due to its small size. Therefore, we used the methyl-TROSY combined with spin-labeling to investigate the structure of the complex [35, 36] as the molecular

weight of the cTAF-1β-gH1.10 complex is too large for its structural determination by conventional NMR. We first assigned the methyl groups of the Ile, Leu, and Val residues of gH1.10 in the free form using three-dimensional NMR spectroscopy with double (^{15}N, ^{13}C)-labeled proteins and specific mutations (Fig. S2). Next, we assigned the methyl groups of gH1.10 in complex with cTAF-1β by overlaying the ^{1}H-^{13}C TROSY spectra of the free gH1.10 and that bound to the cTAF-1β (Fig. 2A, Fig. S2), using the samples that have the methyl groups of Ile, Leu and Val in gH1.10 labeled with ^{1}H and ^{13}C while replacing all other protons with deuterium.

The crystal structure of the dimeric cTAF-1β (PDB ID: 2E50) is asymmetric. However, the dimeric protein displayed only one set of backbone peaks in the ^{1}H-^{15}N TROSY spectrum, suggesting that it has a symmetric structure in solution and crystal packing might contribute to the asymmetry (Fig. S3). Therefore, we used Xplor-NIH's strict symmetry facility to generate a symmetric solution structure of cTAF-Iβ starting from the crystal structure for later modeling study (Fig. 2B) (see Methods). We chose four sites (37, 62, 140, and 152) on the surface of cTAF-1β for spin labeling with S-(2,2,5,5-tetramethyl-2,5-dihydro-1H-pyrrol-3-yl) methyl methanethiosulfonate (MTSL) (Fig. 2B). The spin labels at positions 37 and 152 had larger effects on the peak intensities for the methyl groups of gH1.10, whereas the spin labels at 62 and 140 only led to small effects (Fig. 2C). For the spin labels at 37 and 152 positions, we converted the intensity ratios (I_{oxi}/I_{red}) of the methyl peaks, with oxidized and reduced MTSL, respectively, to distances between the paramagnetic oxygen atoms of MTSL and the methyl carbons in gH1.10 using an empirical correlation derived from spin-label studies on cTAF-1β alone (Fig. S3).

Structural modeling of the gH1.10-cTAF-1β complex

For structural modeling of the gH1.10-cTAF-1β complex, we used the HADDOCK program to dock one gH1.10 to the dimeric cTAF-1β with the distance restraints obtained from the spin labels in one monomer of cTAF-Iβ. A low-energy conformation was chosen for molecular dynamics simulation in the presence of water molecules, leading to the final model of the gH1.10-cTAF-1β complex (Fig. 2D). The distances obtained from these spin-label experiments and those calculated from the structure model showed a good correlation (Fig. 2E). We note that the effects of the spin labels from the other monomer of cTAF-1β were ignored in our calculations, which is consistent with the final structural model as the distances between these spin labels and the methyl groups in gH1.10 are larger than 25 Å. The structure model shows that gH1.10 interacts with cTAF-1β mainly through electrostatic interactions (Fig. 3A). We also examined the chemical shift and intensity changes of the methyl groups in gH1.10 due to the binding of cTAF-Iβ. Consistent with the model, we observed that the methyl groups that show large changes in chemical shifts and peak intensities are close to the binding interface (Fig. 3B-D).

Mutation effects on binding affinity and chaperone function

To further verify the structural model, we made Ala-scanning mutations of the positively charged residues in the globular domain of H1.10 and measured the mutation effects on the binding affinity (Fig. 4A-C, Fig. S4 and Table S1). The titration curve fits a 1:1 binding between TAF-Iβ and H1.10 per monomer, consistent with the stoichiometry measured in

the SEC-MALS experiment. It also suggests that the two H1.10 molecules independently bind to the TAF-Iβ dimer. The mutations at the binding interface reduced the binding affinity substantially. In contrast, the H1.10 mutations away from the binding interface showed minor effects. Similarly, the interface mutations in cTAF-Iβ showed larger effects on the binding affinity, whereas mutations at sites away from the interface showed negligible effects (Fig. 4D, E and Fig. S5).

Overlay of the globular domains of H1.10 in the chromatosome structure [21] and in the gH1.10-cTAF-Iβ complex reveals that cTAF-Iβ clashes with the linker DNA (Fig. 5A), suggesting that TAF-Iβ inhibits binding of H1.10 to the nucleosome. Indeed, in the gel shift experiments, we found that TAF-Iβ can evict H1.10 in the chromatosome and the mutations that reduced the binding affinity also decreased the capability of TAF-Iβ to remove H1.10 from the chromatosome (Fig. 5C).

Discussion

In this study, we established a structural model for the cTAF-Iβ-gH1.10 complex by using the distance constraints obtained from spin labeling-methyl-TROSY NMR studies and docking calculation. The model is further supported by the chemical shift perturbations, NMR peak intensity changes, and the effects of mutations on the binding affinities between H1.10 and TAF-Iβ. In the model, cTAF-Iβ and gH1.10 interact primarily through electrostatic interactions. Since the charge distribution of the globular domain is similar among the somatic linker histone isoforms [37], it is likely that TAF-Iβ binds to other linker histone isoforms in a similar manner. Also, we find that TAF-Iβ binding of H1.10 blocks the linker histone sites that interact with linker DNA in the chromatosome, revealing that TAF-Iβ functions as a chaperone by preventing the interactions between linker DNA and the linker histone, a mechanism that is commonly used by the core histone chaperones [38-40]. In addition, from our model, we find that the highly positively charged intrinsically disordered C-terminal tail of H1.10 is close to the highly negatively charged intrinsically disordered C-terminal tails of TAF-Iβ (Fig. 5B), suggesting that TAF-Iβ and H1.10 form electrostatic interactions through both the folded and intrinsically disordered regions.

Our results show that the paradoxical behavior of TAF-Iβ can be explained in terms of its concentration. At lower concentrations, TAF-Iβ may help linker histone incorporation into the nucleosome to form the chromatosome by preventing aggregation of linker histone onto DNA, which inactivates transcription. At higher concentrations, TAF-Iβ can help evacuate linker histones from chromatin by shifting the equilibrium toward the linker histone-TAF-Iβ complex, which activates transcription. We note that a recent study also showed that it took ~10^4 fold of excess ProTα chaperone to compete with the nucleosome for binding of the linker histone H1.0 [41]. We speculate that the local concentration of the chaperones inside the cell may be regulated by other mechanisms such as liquid-liquid phase separation.

The equilibrium dissociation constant, Kd, for the full-length H1.10 and TAF-Iβ, measured by ITC in our study, is about 10 times smaller than that between the fully intrinsically disordered ProTα and the linker histone H1.0, ~50 nM [42] versus ~500 nM (Table S1). However, these Kd values are several orders of magnitudes larger than the Kd value (~2 pM)

measured by the single-molecule fluorescence resonance energy transfer (smFRET) method for ProTα and H1.0 [28, 42]. Recently, it has been speculated that the relatively lower affinity measured by ITC might be caused by the formation of the trimeric complex (two ProTα bind one H1.0) [43, 44]. However, to reach a population of ~50% for the trimeric species, the ratio of the chaperone versus linker histone needs to be 100-fold higher [43]. In the protein concentration range used in the ITC experiment (<1 μM), the chaperone-linker histone complex exists predominantly as a dimer with the measured stoichiometry close to 1:1 [42]. Moreover, NMR titration data also showed that ProTα binds to the linker histone in 1:1 stoichiometry at even higher concentrations (11-44 μM)[28]. Furthermore, the more recent study showed that it took ~10^4 fold of excess ProTα chaperone to compete with the nucleosome for binding of the linker histone[41], indicating that ProTα does not bind the linker histone with ultrahigh affinity.

Finally, we note that the gH1.10-cTAF-Iβ complex is resistant to crystallization. It is too small for cryo-EM studies but too large for conventional NMR. Also, in comparison with our model, the structure of the gH1.10-cTAF-Iβ complex predicted by alphafold2 shows a very different orientation despite a similar location of gH1.10 relative to the cTAF-Iβ dimer (Fig. S6). Thus, our study demonstrates that methyl-TROSY NMR combined with spin-labeling can be useful for obtaining structural information of protein complexes of similar sizes, providing insights into their biological functions.

Materials and Methods

Gene cloning, protein expression, and purification

The genes that encode full-length TAF-Iβ and linker histone H1.10 were synthesized and cloned into pET15b expression vectors (Biobasic.com, Canada) with His-tags and Thrombin cutting site at N-terminus for TAF-Iβ (MGSSHHHHHHSSGLVPRGSH-TAF-1β) and His-tags at C-terminus for H1.10 (H1.10-HHHHHH). The folded core region of TAF-Iβ (cTAF-Iβ) including the N-terminal tag MGSSHHHHHHSSGLVPRGSH-TAF-1β(21-224) was made by adding a stop codon after residue 224. The globular domain of H1.10 (gH1.10, 41-120) was cloned into pET28b with His-tag and HRV-3C cutting site at the N-terminus. The mutants of TAF-Iβ and H1.10 were made using quick change kit. They were confirmed by DNA sequencing (Genewiz, USA). For the proteins used in all experiments, their removable His-tags were cut off.

Proteins were expressed in E-coli BL-21-CodonPlus (DE3)-RIPL competent cells (Agilent, USA) at 37 °C in LB media for non-labeled proteins. To make $^{15}N/^{13}C$-labeled linker histone H1.10 and TAF-Iβ, *Escherichia coli* BL21-CodonPlus (DE3)-RIPL competent cells (Agilent) were transformed with corresponding plasmids and grown at 37 °C in LB media to an OD600 of 1.0. The cells were pelleted by centrifugation, resuspended in fresh M9 media supplemented with 1g/L $^{15}NH_4Cl$ as the only nitrogen source and with 2g/L of ^{13}C- and/or ^{2}H glucose as the only carbon source. After growing in M9 medium for 30 minutes, 0.5 mM IPTG was added to induce expression and the cells were grown at 37 °C for 4-5 hours and harvested using centrifugation. ^{13}C-methyl-labeling of Ile, Leu, Val residues was made by adding the methyl during protein expression following the published protocol [45].

To purify linker histone H1.10, cells from 1 liter of grown medium were resuspended in 40 mL lysis buffer (50 mM NaH_2PO_4/Na_2HPO_4, pH 8.0, 500 mM NaCl, 6M guanidine hydrochloride) and lysed by sonication. The clarified lysate was added to the column with 5 mL of complete™ His-Tag Purification Resin (Roche) equilibrated with buffer (50 mM NaH_2PO_4/Na_2HPO_4, pH 8.0, 500 mM NaCl, 10 mM imidazole, 6 M guanidine hydrochloride). After gentle stirring 2 hours at room temperature, the beads were washed with 50 mL of 4M urea wash buffer first, then washed by 200 mL wash buffer (50 mM NaH_2PO_4/Na_2HPO_4, pH 8.0, 500 mM NaCl, 10 mM imidazole). Proteins were eluted with elution buffer (50 mM NaH_2PO_4/Na_2HPO_4, pH 8.0, 500 mM NaCl, 250 mM imidazole). The elution was further purified by HPLC with an RP-protein column (YMC) and lyophilized to get protein powder for future use.

To purify TAF-Iβ, cells from 1 liter of grown medium were resuspended in 40 mL lysis buffer (25 mM HEPES, pH 7.9, 500 mM NaCl, 1mM EDTA, 1mM PMSF, 1mL SIGMAFAST Protease inhibitor Cocktail stock solution) and lysed by sonication. The clarified lysate was concentrated to 15 mL and precipitated by adding 3.75 g ammonium sulfate. The supernatants were added to the column with 5 mL of cOmplete™ His-Tag Purification Resin (Roche) equilibrated with wash buffer (25 mM NaH_2PO_4/Na_2HPO_4, pH 8.0, 500 mM NaCl, 10 mM imidazole). After being incubated for 2 hours at 4 °C, the beads were washed with 200 ml wash buffer (25 mM NaH_2PO4/Na_2HPO_4, pH 8.0, 500 mM NaCl, 10 mM imidazole). The eluted proteins were further purified using FPLC with HiLoad 16/60 Superdex 75 prep grade gel filtration column (GE). The purity of the proteins was checked using SDS gel. To make samples with spin labels, TAF-Iβ Cys mutations (E37C, K62C, S140C, or S152C) were made. MTSL (S-(2,2,5,5-tetramethyl-2,5-dihydro-1H-pyrrol-3-yl)methyl methanethiosulfonate) was linked to Cys of the corresponding purified TAF-Iβ mutant following the earlier protocol[46].

Molecular weight measurement by SEC-MALS

SEC-MALS (WYATT Technology) is connected to FPLC (AKTA PURE, GE) and equipped with Superdex 200 Increase 10/300 GL column (Cytiva). The concentrations of protein samples are ~100 to 120 uM. The SEC-MALS instrument was pre-equilibrated overnight with PBS buffer at pH 7.4 and a flow rate of 0,3 ml/min. The SEC-MALS was further washed with five volumes of the same buffer for each run before the injection of protein samples.

Binding affinity measurement by ITC

All proteins for binding affinity measurements were purified using AKTA FPLC with Superdex 75 Increase 10/300 GL column (GE Healthcare) equilibrated with PBS buffer prior to the ITC experiment. Protein concentrations were determined by measuring absorbance at 280 nm with a NanoDrop DS-11FX+ spectrophotometer (DeNovix). ITC experiments were performed using a MicroCal PEAQ-ITC calorimeter at 20 °C with a stirring rate of 750 rpm. The injection volume was 2μl with an injection interval of 150s for a total of 19 injections. ITC data were analyzed with MicroCal PEAQ-ITC analysis software to obtain the binding stoichiometry (N), dissociation constant (K_d), and enthalpy change (ΔH) for the binding of H1.10 and TAF-Iβ and their mutants (Table S1).

NMR experiments

All NMR samples of $^{2}H/^{15}N/1^{3}C$-labelled cTAF-Iβ, $^{15}N/^{13}C$ or ^{15}N/(Ile, Leu, Val) methyl-labelled gH1.10 were prepared in the buffer of 10 mM MES, 50 mM NaCl, pH 6.3. The backbone and/or side-chain chemical shift assignments were made by collecting the standard triple-resonance 3D experiments NMR spectra on Bruker 700 and 900 MHz NMR instruments equipped with cryo-probes. The multi-dimensional NMR spectra were processed with NMRPipe[47] and SMILE[48] and analyzed by NMRViewJ[49]. The peak intensities of the well-separated peaks in the ^{1}H-^{15}N HSQC/TROSY or ^{1}H-^{13}C HMQC spectra were measured using NMRViewJ. Chemical shift perturbations (CSP) were calculated using the following equations: $CSP = (0.5((\Delta^{1}H)^{2} + 0.14(\Delta^{15}N)^{2}))^{-2}$ for ^{1}H-^{15}N and $CSP = (0.5((\Delta^{1}H)^{2} + 0.30(\Delta^{13}C)^{2}))^{-2}$ for ^{1}H-^{13}C.

Spin label effects (I_{oxi}/I_{red}) were evaluated by the peak intensity ratio of oxidized form to a reduced form of the gH1.10. To obtain the distance dependence on spin label effects, an empirical curve was generated by fitting the peak intensity ratio of oxidized form to the reduced form of cTAF-Iβ E37CMTSL versus the distance between the oxygen atom of MTSL and the amide hydrogen in the structure of cTAF-Iβ, which were measured manually using PyMol (The PyMOL Molecular Graphics System, Version 2.1, Schrödinger, LLC.). We used an empirical relationship between I_{oxi}/I_{red} and the distance derived from spin-label studies on the free cTAF-Iβ (Fig. S3).

Model building

Xplor-NIH's strict symmetry facility [50] was used to generate a solution structure of cTAF-Iβ starting from the crystal structure coordinates in PDB ID 2E50. In this calculation, coordinates missing in the reference structure were added and an NCS program restrained the backbone atomic coordinates to those in the reference structure's regular regions (residues 24-76, 82-106, and 109-154). The following data were used in this calculation: hydrogen-bonding distance restraints, and TALOS-generated dihedral angle restraints[51]. Standard torsion angle and hydrogen-bonding database terms were used along with those for bonds, bond angles, improper, and RepelPot to prevent atomic overlap. A weighted sum of these energy terms was used in a standard molecular dynamics simulated annealing protocol resulting in a structure that agreed with the crystal reference structure to within 3.2 Å RMSD for the Cα atoms in the regular regions defined above. The NMR structure (2LSO) [33] of gH1.10 was used as it is. The model structures of cTAF-Iβ-gH1.10 complex were calculated via HADDOCK Web Server (HADDOCK 2.4)[52] with the distance restraints derived from our spin-label studies. A low-energy conformation was chosen for molecular dynamics simulation in the presence of water molecules, leading to the final model of the gH1.10-cTAF-1β complex.

Chaperone function assay

The 197 bp W601 nucleosome was reconstituted according to the previous protocol[53]. H1.10 chromatosome was reconstituted by mixing 2 μM H1.10 with 2 μM nucleosome in the binding buffer (10 mM Tris-HCl, 1 mM EDTA, 10 mM NaCl, and 1 mM DTT) and incubated on ice for 30 minutes. To test the chaperone function of TAF-Iβ, TAF-Iβ and its mutants at various concentrations (1.0, 5.0, 10.0, or 15.0 μM) were mixed with

0.1 μM H1.10 chromatosome with equal volume (10 μL each) in the binding buffer. The solutions were incubated at 37°C for 30 min. After the addition of 2% of Ficoll 6000, H1.10 chromatosome and free nucleosome were resolved by electrophoresis at 100V for 2h using 5% native PAGE gel in 0.2X TBE. The gel was stained with Midori Green Advance (Bulldog Bio) and visualized using ChemiDoc Imager (Bio-Rad). Band intensities were measured using ImageJ [54]. Three replicates were performed.

Supplementary Material

Refer to Web version on PubMed Central for supplementary material.

Acknowledgement

We thank Jinfa Ying for assistance of the use of 900 MHz NMR instrument. This work was supported by the intramural research program of National Institutes of Health and used NIH high performance computing Biowulf system for structural calculations.

Data availability

The chemical shifts from this study have been deposited to BMRB with an ID of 51409.

References

[1]. Kornberg RD. Chromatin structure: a repeating unit of histones and DNA. Science. 1974;184:868–71. [PubMed: 4825889]

[2]. Kornberg RD, Thomas JO. Chromatin structure; oligomers of the histones. Science. 1974;184:865–8. [PubMed: 4825888]

[3]. Olins AL, Olins DE. Spheroid chromatin units (v bodies). Science. 1974;183:330–2. [PubMed: 4128918]

[4]. Fyodorov DV, Zhou BR, Skoultchi AI, Bai Y. Emerging roles of linker histones in regulating chromatin structure and function. Nat Rev Mol Cell Biol. 2018;19:192–206. [PubMed: 29018282]

[5]. Hergeth SP, Schneider R. The H1 linker histones: multifunctional proteins beyond the nucleosomal core particle. EMBO Rep. 2015;16:1439–53. [PubMed: 26474902]

[6]. Fan Y, Nikitina T, Zhao J, Fleury TJ, Bhattacharyya R, Bouhassira EE, et al. Histone H1 depletion in mammals alters global chromatin structure but causes specific changes in gene regulation. Cell. 2005;123:1199–212. [PubMed: 16377562]

[7]. Shen X, Gorovsky MA. Linker histone H1 regulates specific gene expression but not global transcription in vivo. Cell. 1996;86:475–83. [PubMed: 8756729]

[8]. Maresca TJ, Freedman BS, Heald R. Histone H1 is essential for mitotic chromosome architecture and segregation in Xenopus laevis egg extracts. J Cell Biol. 2005;169:859–69. [PubMed: 15967810]

[9]. Lee H, Habas R, Abate-Shen C. MSX1 cooperates with histone H1b for inhibition of transcription and myogenesis. Science. 2004;304:1675–8. [PubMed: 15192231]

[10]. Zhang Y, Cooke M, Panjwani S, Cao K, Krauth B, Ho PY, et al. Histone h1 depletion impairs embryonic stem cell differentiation. PLoS Genet. 2012;8:e1002691. [PubMed: 22589736]

[11]. Lu X, Wontakal SN, Kavi H, Kim BJ, Guzzardo PM, Emelyanov AV, et al. Drosophila H1 regulates the genetic activity of heterochromatin by recruitment of Su(var)3-9. Science. 2013;340:78–81. [PubMed: 23559249]

[12]. Christophorou MA, Castelo-Branco G, Halley-Stott RP, Oliveira CS, Loos R, Radzisheuskaya A, et al. Citrullination regulates pluripotency and histone H1 binding to chromatin. Nature. 2014;507:104–8. [PubMed: 24463520]

[13]. Willcockson MA, Healton SE, Weiss CN, Bartholdy BA, Botbol Y, Mishra LN, et al. H1 histones control the epigenetic landscape by local chromatin compaction. Nature. 2021; 589:293–8. [PubMed: 33299182]

[14]. Torres CM, Biran A, Burney MJ, Patel H, Henser-Brownhill T, Cohen AS, et al. The linker histone H1.0 generates epigenetic and functional intratumor heterogeneity. Science. 2016;353:1514–25.

[15]. Yusufova N, Kloetgen A, Teater M, Osunsade A, Camarillo JM, Chin CR, et al. Histone H1 loss drives lymphoma by disrupting 3D chromatin architecture. Nature. 2021; 589:299–305. [PubMed: 33299181]

[16]. Duffney LJ, Valdez P, Tremblay MW, Cao X, Montgomery S, McConkie-Rosell A, et al. Epigenetics and autism spectrum disorder: A report of an autism case with mutation in H1 linker histone HIST1H1E and literature review. Am J Med Genet B Neuropsychiatr Genet. 2018;177:426–33. [PubMed: 29704315]

[17]. Flex E, Martinelli S, Van Dijck A, Ciolfi A, Cecchetti S, Coluzzi E, et al. Aberrant Function of the C-Terminal Tail of HIST1H1E Accelerates Cellular Senescence and Causes Premature Aging. Am J Hum Genet. 2019;105:493–508. [PubMed: 31447100]

[18]. Happel N, Doenecke D. Histone H1 and its isoforms: contribution to chromatin structure and function. Gene. 2009;431:1–12. [PubMed: 19059319]

[19]. Allan J, Hartman PG, Crane-Robinson C, Aviles FX. The structure of histone H1 and its location in chromatin. Nature. 1980;288:675–9. [PubMed: 7453800]

[20]. Singer DS, Singer MF. Studies on the interaction of H1 histone with superhelical DNA: characterization of the recognition and binding regions of H1 histones. Nucleic Acids Res. 1976;3:2531–47. [PubMed: 186761]

[21]. Zhou BR, Feng H, Kale S, Fox T, Khant H, de Val N, et al. Distinct Structures and Dynamics of Chromatosomes with Different Human Linker Histone Isoforms. Mol Cell. 2021;81:166–82 e6. [PubMed: 33238161]

[22]. Allan J, Mitchell T, Harborne N, Bohm L, Crane-Robinson C. Roles of H1 domains in determining higher order chromatin structure and H1 location. J Mol Biol. 1986;187:591–601. [PubMed: 3458926]

[23]. Hammond CM, Stromme CB, Huang H, Patel DJ, Groth A. Histone chaperone networks shaping chromatin function. Nat Rev Mol Cell Biol. 2017;18:141–58. [PubMed: 28053344]

[24]. George EM, Brown DT. Prothymosin alpha is a component of a linker histone chaperone. FEBS Lett. 2010;584:2833–6. [PubMed: 20434447]

[25]. Kato K, Okuwaki M, Nagata K. Role of Template Activating Factor-I as a chaperone in linker histone dynamics. J Cell Sci. 2011;124:3254–65. [PubMed: 21940793]

[26]. Shintomi K, Iwabuchi M, Saeki H, Ura K, Kishimoto T, Ohsumi K. Nucleosome assembly protein-1 is a linker histone chaperone in Xenopus eggs. Proc Natl Acad Sci U S A. 2005;102:8210–5. [PubMed: 15928086]

[27]. Finn RM, Browne K, Hodgson KC, Ausio J. sNASP, a histone H1-specific eukaryotic chaperone dimer that facilitates chromatin assembly. Biophys J. 2008;95:1314–25. [PubMed: 18456819]

[28]. Borgia A, Borgia MB, Bugge K, Kissling VM, Heidarsson PO, Fernandes CB, et al. Extreme disorder in an ultrahigh-affinity protein complex. Nature. 2018;555:61–6. [PubMed: 29466338]

[29]. Matsumoto K, Nagata K, Ui M, Hanaoka F. Template activating factor I, a novel host factor required to stimulate the adenovirus core DNA replication. J Biol Chem. 1993;268:10582–7. [PubMed: 8486711]

[30]. von Lindern M, van Baal S, Wiegant J, Raap A, Hagemeijer A, Grosveld G. Can, a putative oncogene associated with myeloid leukemogenesis, may be activated by fusion of its 3' half to different genes: characterization of the set gene. Mol Cell Biol. 1992;12:3346–55. [PubMed: 1630450]

[31]. Seo SB, McNamara P, Heo S, Turner A, Lane WS, Chakravarti D. Regulation of histone acetylation and transcription by INHAT, a human cellular complex containing the set oncoprotein. Cell. 2001;104:119–30. [PubMed: 11163245]

[32]. Kawase H, Okuwaki M, Miyaji M, Ohba R, Handa H, Ishimi Y, et al. NAP-I is a functional homologue of TAF-I that is required for replication and transcription of the adenovirus genome in a chromatin-like structure. Genes Cells. 1996;1:1045–56. [PubMed: 9077453]

[33]. Muto S, Senda M, Akai Y, Sato L, Suzuki T, Nagai R, et al. Relationship between the structure of SET/TAF-Ibeta/INHAT and its histone chaperone activity. Proc Natl Acad Sci U S A. 2007;104:4285–90. [PubMed: 17360516]

[34]. Zhang Q, Giebler HA, Isaacson MK, Nyborg JK. Eviction of linker histone H1 by NAP-family histone chaperones enhances activated transcription. Epigenetics Chromatin. 2015;8:30–46. [PubMed: 26339295]

[35]. Tugarinov V, Hwang PM, Kay LE. Nuclear magnetic resonance spectroscopy of high-molecular-weight proteins. Annu Rev Biochem. 2004;73:107–46. [PubMed: 15189138]

[36]. Kato H, van Ingen H, Zhou BR, Feng H, Bustin M, Kay LE, et al. Architecture of the high mobility group nucleosomal protein 2-nucleosome complex as revealed by methyl-based NMR. Proc Natl Acad Sci U S A. 2011;108:12283–8. [PubMed: 21730181]

[37]. Zhou BR, Jiang J, Feng H, Ghirlando R, Xiao TS, Bai Y. Structural Mechanisms of Nucleosome Recognition by Linker Histones. Mol Cell. 2015;59:628–38. [PubMed: 26212454]

[38]. English CM, Adkins MW, Carson JJ, Churchill ME, Tyler JK. Structural basis for the histone chaperone activity of Asf1. Cell. 2006;127:495–508. [PubMed: 17081973]

[39]. Zhou Z, Feng H, Zhou BR, Ghirlando R, Hu K, Zwolak A, et al. Structural basis for recognition of centromere histone variant CenH3 by the chaperone Scm3. Nature. 2011;472:234–7. [PubMed: 21412236]

[40]. Zhou Z, Feng H, Hansen DF, Kato H, Luk E, Freedberg DI, et al. NMR structure of chaperone Chz1 complexed with histones H2A.Z-H2B. Nat Struct Mol Biol. 2008;15:868–9. [PubMed: 18641662]

[41]. Heidarsson PO, Mercadante D, Sottini A, Nettels D, Borgia MB, Borgia A, et al. Release of linker histone from the nucleosome driven by polyelectrolyte competition with a disordered protein. Nat Chem. 2022;14:224–31. [PubMed: 34992286]

[42]. Feng H, Zhou BR, Bai Y. Binding Affinity and Function of the Extremely Disordered Protein Complex Containing Human Linker Histone H1.0 and Its Chaperone ProTalpha. Biochemistry. 2018;57:6645–8. [PubMed: 30430826]

[43]. Sottini A, Borgia A, Borgia MB, Bugge K, Nettels D, Chowdhury A, et al. Polyelectrolyte interactions enable rapid association and dissociation in high-affinity disordered protein complexes. Nat Commun. 2020;11:5736–49. [PubMed: 33184256]

[44]. Schuler B, Borgia A, Borgia MB, Heidarsson PO, Holmstrom ED, Nettels D, et al. Binding without folding - the biomolecular function of disordered polyelectrolyte complexes. Curr Opin Struct Biol. 2020;60:66–76. [PubMed: 31874413]

[45]. Tugarinov V, Kanelis V, Kay LE. Isotope labeling strategies for the study of high-molecular-weight proteins by solution NMR spectroscopy. Nat Protoc. 2006;1:749–54. [PubMed: 17406304]

[46]. Zhou BR, Feng H, Kato H, Dai L, Yang Y, Zhou Y, et al. Structural insights into the histone H1-nucleosome complex. Proc Natl Acad Sci U S A. 2013;110:19390–5. [PubMed: 24218562]

[47]. Delaglio F, Grzesiek S, Vuister GW, Zhu G, Pfeifer J, Bax A. NMRPipe: a multidimensional spectral processing system based on UNIX pipes. J Biomol NMR. 1995;6:277–93. [PubMed: 8520220]

[48]. Ying J, Delaglio F, Torchia DA, Bax A. Sparse multidimensional iterative lineshape-enhanced (SMILE) reconstruction of both non-uniformly sampled and conventional NMR data. J Biomol NMR. 2017;68:101–18. [PubMed: 27866371]

[49]. Johnson BA, Blevins RA. NMR View: A computer program for the visualization and analysis of NMR data. J Biomol NMR. 1994;4:603–14. [PubMed: 22911360]

[50]. Schwieters CD, Bermejo GA, Clore GM. Xplor-NIH for molecular structure determination from NMR and other data sources. Protein Sci. 2018;27:26–40. [PubMed: 28766807]

[51]. Cornilescu G, Delaglio F, Bax A. Protein backbone angle restraints from searching a database for chemical shift and sequence homology. J Biomol NMR. 1999;13:289–302. [PubMed: 10212987]

[52]. van Zundert GCP, Rodrigues J, Trellet M, Schmitz C, Kastritis PL, Karaca E, et al. The HADDOCK2.2 Web Server: User-Friendly Integrative Modeling of Biomolecular Complexes. J Mol Biol. 2016;428:720–5. [PubMed: 26410586]

[53]. Zhou BR, Bai Y. Preparation of scFv stabilized chromatosomes for single-particle cryo-EM structure determination. STAR Protoc. 2021;2:100396. [PubMed: 33786462]

[54]. Schneider CA, Rasband WS, Eliceiri KW. NIH Image to ImageJ: 25 years of image analysis. Nat Methods. 2012;9:671–5. [PubMed: 22930834]

Highlights

- Human linker histone isoform H1.10 and its chaperone TAF-Iβ form a 2:2 complex.
- Structure of the H1.10-TAF-Iβ core complex from methyl NMR-spin label studies.
- H1.10 interacts with TAF-Iβ mainly through electrostatic interactions.
- TAF-Iβ functions as a chaperone by blocking the DNA binding sites of H1.10.

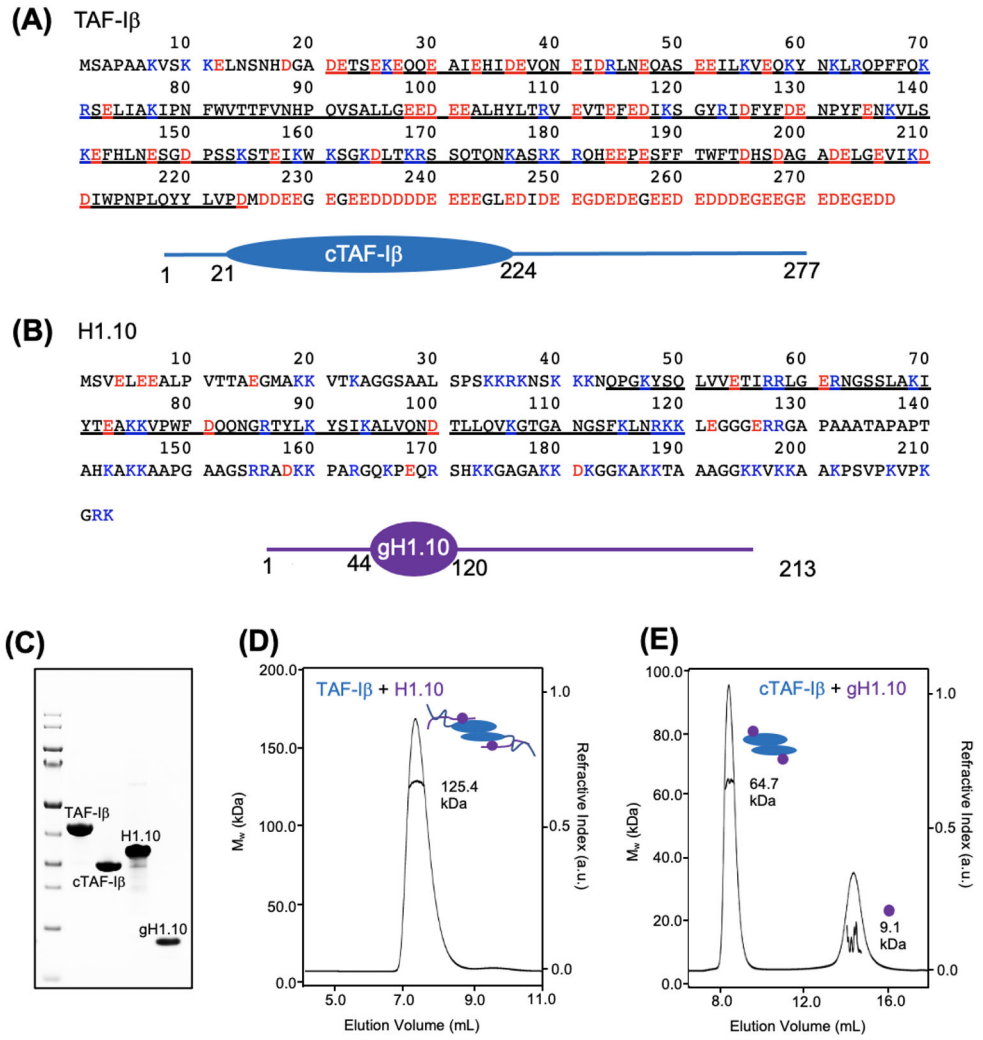

Fig. 1. TAF-Iβ and linker histone H1.10 form a 2:2 tetramer.

(**A** and **B**) Amino acid sequence of TAF-Iβ and H1.10. Positively charged residues are in blue color. Negatively charged residues are in red color. The underline indicates the folded core and globular domain, respectively. (**C**) SDS gels of purified TAF-Iβ (32.2 kDa), cTAF-Iβ (26.3 kDa), H1.10 (23.6 kDa), and gH1.10 (9.5 kDa). (**D** and **E**) SEC-MALS of the TAF-Iβ-H1.10 (~125uM) and cTAF-Iβ-gH1.10 (~100uM) complexes with excess of H1.10 and gH1.10, respectively. The lines within the peak indicate the molecular weights in the peak regions.

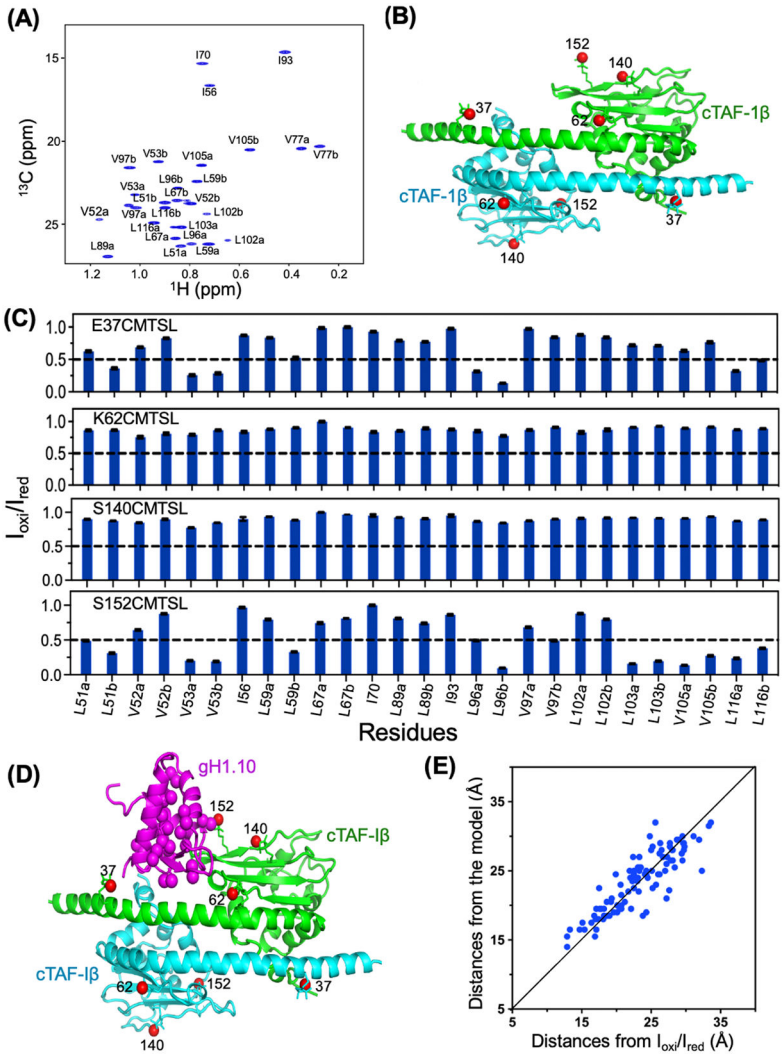

Fig. 2. Structural model of the cTAF-Iβ-gH1.10 complex.

(**A**) NMR spectrum of the Ile, Leu and Val methyl groups in gH1.10 bound to cTAF-Iβ. (**B**) Illustration of the positions labeled with MTSL. (**C**) Ratios of peak intensities of the methyl groups in gH1.10 between oxidized and reduced forms of the MTSL labels at various locations. (**D**) Structural model of the cTAF-Iβ-gH1.10 complex with one gH1.10. (**E**) Correlations between the distances derived from spin-label data and those calculated from the structural model.

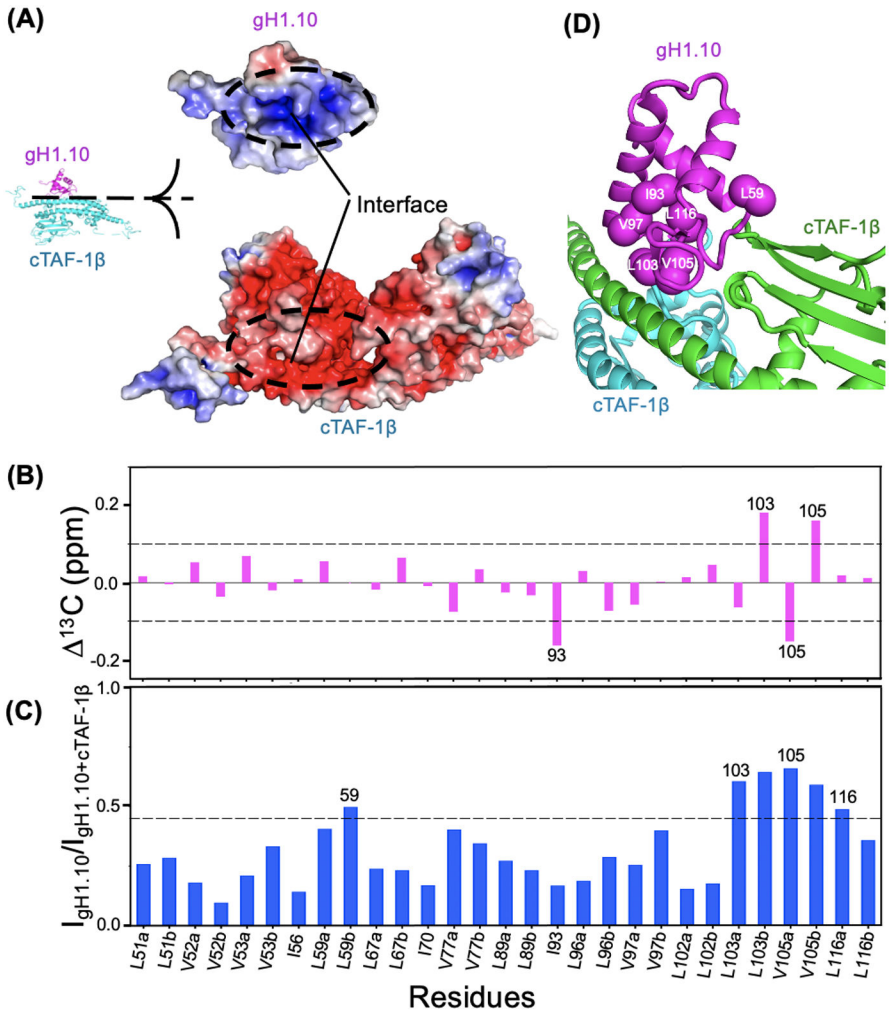

Fig. 3. Electrostatic interactions and effects of cTAF-Iβ binding on the chemical shifts and peak intensities of the gH1.10 methyl groups.

(**A**) Illustration of electrostatic interactions between gH1.10 and cTAF-Iβ. The electrostatic potential range is from −5 eV (red) to +5 eV (blue). (**B**) Methyl-^{13}C chemical shift changes of gH1.10 upon binding of cTAF-Iβ. The dashed line is at 0.1. (**C**) Methyl peak intensity ratios of gH1.10 upon binding of cTAF-Iβ. The dashed line is at 0.45. (**D**) Illustration of methyl groups that show large changes in (**B**) and (**C**).

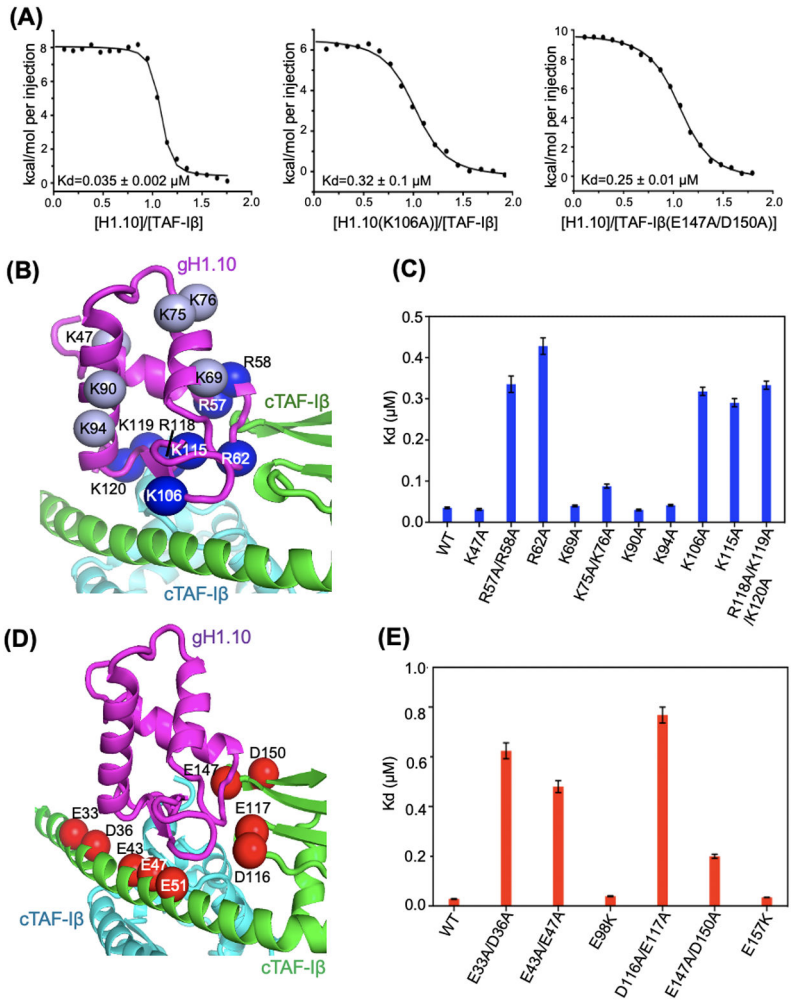

Fig. 4. Effects of mutations on the binding affinity between TAF-Iβ and H1.10.

(**A**) Typical ITC titration curves. (**B**) Illustration of positively charged residues in gH1.10. The residues in light and dark blue have small and large effects, respectively, on binding affinity when mutated to Ala (see **C**). (**C**) Summary of the ITC results for the Ala scanning mutations of the positively charged residues in the globular domain of H1.10. Each bar represents the average value from two independent experiments. (**D**) Illustration of negatively charged residues in cTAF-Iβ that are close to gH1.0. (**E**) Summary of the ITC results for the Ala mutations of the negatively charged residues in cTAF-Iβ. Each bar represents the average value from two independent experiments. E98 and E157 are not at the interface and were out of the region shown in (**D**).

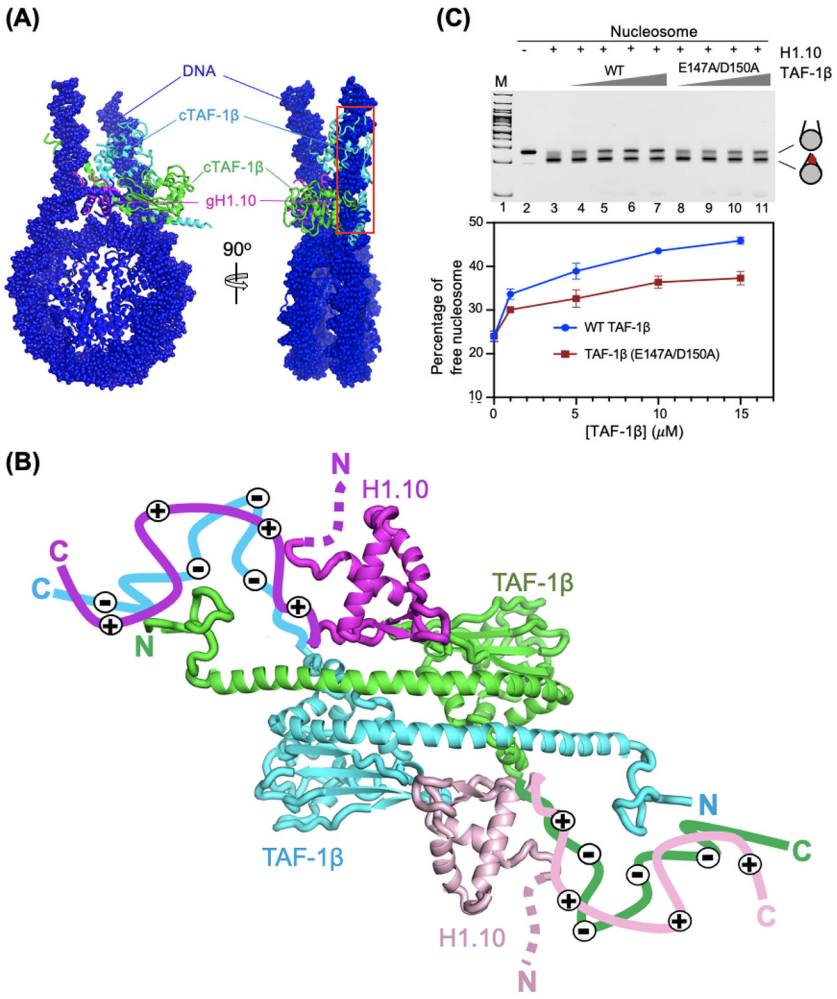

Fig. 5. TAF- Iβ chaperone function assay.

(**A**) Two different views of the overlay of the globular domain of H1.10 in the structures of the chromatosome (PDB ID: 7K60) and cTAF-Iβ-gH1.10. The main clashed region between cTAF-Iβ and the linker DNA is highlighted by the box in red. (**B**) Illustration of the overall structural model of the TAF-Iβ-H1.10 complex. The charged C-terminal tails of TAF-Iβ and H1.10 are shown with lines. The multiple "−" and "+" signs indicate they are negatively and positively charged, respectively. (**C**) Eviction of H1.10 from the chromatosome by TAF-Iβ and the effect of its mutation (E147A/D150A). 0.1 μM nucleosome and H1.10 chromatosome was mixed with TAF-Iβ (lanes: 4-7) and its mutant (lanes 8-11) at 1.0, 5.0, 10.0 or 15.0 μM with equal volume. M: DNA marker. Lane 1: free nucleosome. Lane 2: free chromatosome.